PERFORMANCE EVALUATION OF THE FREQUENCY-DOMAIN DORT IMAGING METHOD WITH UWB RADAR FOR A FINITE-SIZED TARGET

Takuya Sakamoto and Toru Sato

Graduate School of Informatics, Kyoto University
Department of Communications and Computer Engineering
Yoshida-Honmachi, Sakyo-ku, Kyoto 606-8501, Japan

ABSTRACT

Ultra wide-band (UWB) radar imaging systems are a promising field of research as they cover a variety of applications. Among all UWB radar imaging methods, the time-reversal (TR) method enables high-resolution imaging in a multipath environment. Conventional TR methods have been applied to antenna array systems while our previous work proposed a type of TR method, namely the frequency-domain Décomposition de Opérateur de Retournement Temporel (DORT) method, designed for a low-cost single antenna-based system. Because the frequency-domain DORT method was developed assuming a point-like target, the performance of the method for a finite-sized target is unknown. In this study, we investigate numerically the performance of the frequency-domain DORT method by applying it to finite-sized targets and evaluating the quality of the resultant images.

***Index Terms*—** ultra wide-band radar, frequency-domain, DORT, multi-path, time-reversal

1. INTRODUCTION

Ultra wide-band (UWB) radar is a promising technology for a variety of applications including surveillance systems. A cost-effective UWB radar system that can be practically applied to a system is needed. Time-reversal (TR), a UWB radar imaging method, has been considered attractive for realizing high-resolution imaging [1]. It is known that TR achieves super-resolution that is much higher than the classical resolution limit determined by the antenna aperture size. To improve the resolution of the TR method, the Décomposition de Opérateur de Retournement Temporel (DORT) method was developed by Devaney et al. [2]. DORT achieves high-resolution capability by separating multiple propagation paths. It achieves this by applying singular value decomposition (SVD) to a matrix produced using a bi-static measurement with an array antenna [3, 4].

In applying the DORT to actual security systems, it is essential to simplify the system and lower the cost; specifically, the number of antennas must be reduced. Sakamoto and Sato [5] extended the original DORT so that it can be applied to a simple system with a single antenna. This method generates the matrix to be decomposed by SVD only in the frequency domain; the method is called a frequency-domain DORT. It has been established that the frequency-domain DORT achieves high-resolution for a point-like target [5]. The performance of the frequency-domain DORT has not been determined for a finite-sized target. To investigate its feasibility in practice, it is necessary to evaluate the imaging performance of the method for targets of various sizes. In this paper we numerically evaluate the relationship between the target size and the imaging quality.

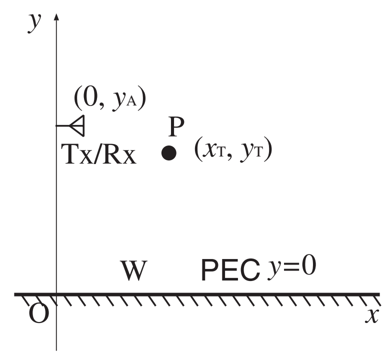

Fig. 1. System model.

2. SYSTEM MODEL

Figure 1 shows the system model assumed in this study, in which a 2-dimensional system with a transverse magnetic (TM) wave is used to estimate the 2-dimensional position of a metallic target. The received signals are calculated using the finite difference time domain (FDTD), with a 6-layered perfect matched layer (PML) for absorbing boundaries and a grid size of 1.0 mm.

Propagation and scattering are numerically calculated for imaging in the DORT. The Green's function for a 2-dimensional scalar wave is expressed using a Hankel function of the first kind. Scattering by a point target is modeled with the Born approximation. This system is composed of a transmit antenna Tx, a receiving antenna Rx, a plate W made of perfectly electric conductor (PEC), and a point-like PEC target P. The transmitted pulse is a UWB pulse $s_{\mathrm{T}}(t)$, which is a mono-cycle pulse in the numerical simulation. We assume that the relative locations of the antennas and the plate are known. The direct wave $s_{\mathrm{D}}(t)$ from Tx to Rx without scattering, as well as the reflected wave $s_{\mathrm{W}}(t)$ from plate W are measured and stored in memory prior to the actual measurement of the targets. Waveforms $s_{\mathrm{D}}(t)$ and $s_{\mathrm{W}}(t)$ are subtracted from a received signal $s_0(t)$ as $s(t) = s_0(t) - s_{\mathrm{D}}(t) - s_{\mathrm{W}}(t)$.

3. FREQUENCY-DOMAIN DORT

$S_1, \cdots, S_N$ are defined as the values of the received signal $S(\omega)$ in the frequency domain at $\omega_1, \cdots, \omega_N$. The matrix K_{FF} is defined as

$$K_{\mathrm{FF}} = \begin{bmatrix} S_1 & S_2 & \cdots & S_L \\ S_{L+1} & S_{L+2} & \cdots & S_{2L} \\ \vdots & \vdots & \vdots & \vdots \\ S_{N-L+1} & S_{N-L+2} & \cdots & S_N \end{bmatrix}, \quad (1)$$

where the rows and columns correspond to coarse and fine changes in frequencies, respectively. We assume $N = L^2$ for simplicity. The Green's function is expressed approximately as a product of two factors, the coarse and fine frequencies. With this approximation, the Green's function for each propagation path can be divided into the two parts, which forms the basis of the frequency-domain DORT.

First, the frequency-domain DORT applies SVD to K_{FF} as $K_{\mathrm{FF}} = U\Sigma V^{\mathrm{H}}$, where Σ is a diagonal matrix with singular values. The left and right singular matrices correspond to coarse and fine frequencies, respectively. As in the conventional DORT, we adopt small $L - PK$ singular values to estimate noise subspaces, where P is the number of multipaths for each point-like target, and K is the number of targets. In this paper we assume $P = 3$ and $K = 1$. We select left and right singular vectors, $\boldsymbol{u}_{PK+1} \cdots \boldsymbol{u}_N$ and $\boldsymbol{v}_{PK+1} \cdots \boldsymbol{v}_N$, respectively, as the base vectors of the noise subspace and obtain the image from the left singular vectors as

$$I_{\mathrm{L}}(\boldsymbol{x}) = \frac{1}{\displaystyle\sum_{i=PK+1}^{L} \sum_{p=1}^{P} \left|\boldsymbol{u}_i^{\mathrm{H}} \boldsymbol{g}_p(\boldsymbol{x})\right|^2 / \left|\boldsymbol{g}_p(\boldsymbol{x})\right|^2}, \quad (2)$$

where $\boldsymbol{g}_p$ is the L-dimensional vector with values of the Green's function for the p-th path at $\omega_1, \omega_{L+1} \cdots, \omega_{N-L+1}$. Similarly, the image $I_{\mathrm{R}}(\boldsymbol{x})$ can be obtained from the right singular vectors. We obtain the final image by multiplying these as $I_{\mathrm{DORT}}(\boldsymbol{x}) = I_{\mathrm{L}}(\boldsymbol{x}) I_{\mathrm{R}}(\boldsymbol{x})$ [5].

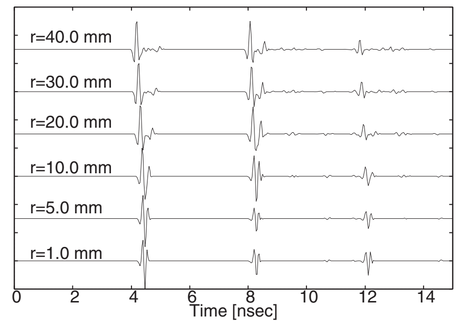

Fig. 2. Received signals.

4. PERFORMANCE EVALUATION OF IMAGING METHODS

The results from applying the conventional TR and the frequency-domain DORT are given in this section. A mono-cycle pulse with a central frequency of 4.0 GHz is transmitted, and the received signals are processed for imaging. As is shown in Fig. 1, the PEC plate is on the x-axis, the antenna is on the y-axis at $(0.0\mathrm{mm}, 600.0\mathrm{mm})$, and the target is at $(600.0\mathrm{mm}, 750.0\mathrm{mm})$. In the proposed method, we set $L = 10$ and $N = 100$ while $L - PK = 7$ small singular values are selected from the 10×10 matrix K_{FF}, and the corresponding seven left and right singular vectors are used for imaging.

For simplicity, the imaging methods are applied to noiseless data. Figure 2 shows the received signals from a cylindrical metallic target with radius r. In the figure, we see three echoes corresponding to the three propagation paths. As the radius becomes larger, the earlier echoes are received. Creeping echoes are also observed for a target with a larger radius. Note that the waveform distortions caused by the larger targets can degrade estimated images because the frequency-domain DORT assumes a Green's function based on Rayleigh scattering with a point target.

Figure 3 shows the image estimated by the conventional TR. For the case with a small r, three waveforms interfere to generate a prominent peak at the correct position. However, the three waveforms do not meet at the same point for a large r, and the maximum peak is shifted to the point where two of them intersect. In addition, we see artifacts caused by creeping waves for a large r. The estimated target position is close to the target boundary for a large r.

Fig. 4 shows the images obtained by the frequency-domain DORT. We see that the images are clear for a small r, while there are residual artifacts and a blurred image for a large r. However the frequency-domain DORT is still able to function and to produce an image even for a relatively large target.

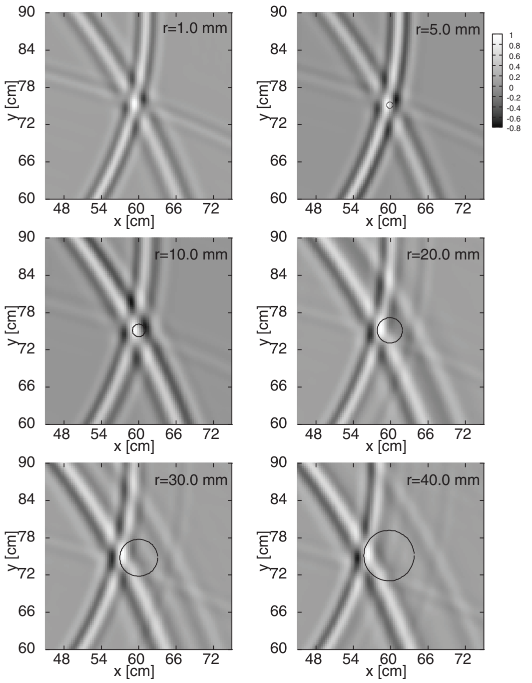

Fig. 3. Images produced by the conventional TR.

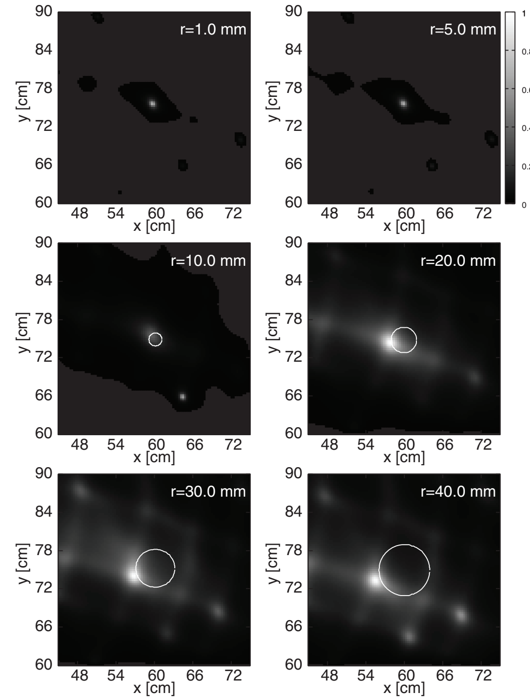

Fig. 4. Images produced by the frequency-domain DORT.

5. EVALUATION OF ACCURACY AND SHARPNESS

Fig. 5 shows the estimation error of a target position for the conventional TR and the frequency-domain DORT. The error is the distance between the estimated position and the point on the target surface that is closest to it. The figure shows that the conventional TR has an error of less than 10.0 mm for any r, while the frequency-domain DORT gives a larger error for a large r. This is because the orthogonality between the noise subspace and the Green's function assumed in the frequency-domain DORT is not satisfied since the point target model is not valid for actual scattering with a finite-sized target. In addition, the waveform distortion including creeping waves, contributes to the degradation of the image. Note that the frequency-domain DORT gives a large error for $r = 10.0$ mm because the maximum point falls upon the false artifact as in Fig. 4.

Finally, we evaluate the sharpness of the images using Muller and Buffington's sharpness metric (MB sharpness) [6]. The p-th order MB sharpness metric h_p is expressed as $h_p = \frac{1}{M}\sum_{m=1}^{M} I_m^p$, where I_m is a vector with elements of the image normalized by the maximum pixel, and M is the number of pixels in the image. The order p shows the order of the statistics, meaning the sharpness of the image for $p > 2$ with higher-order statistics. Note that a small value h_p means a sharp image using this metric. Here, we set $p = 4$ and evaluate the sharpness of the images. Fig. 6 shows the 4-th order MB sharpness metric for each method. The figure shows that the frequency-domain DORT gives high sharpness for a small r, in particular for $r \leq 10.0$ mm. The frequency-domain DORT gives greater sharpness than the conventional TR for $r \leq 70.0$ mm. Conversely, for $r > 70.0$ mm the conventional TR gives greater sharpness. The conventional TR gives an almost unchanged sharpness regardless of r.

6. CONCLUSIONS

We investigated the performance of the frequency-domain DORT, a type of TR method and compared it with the conventional TR method for a target with a variety of sizes. The frequency-domain DORT is a high-resolution radar imaging method, and an extended version of the conventional DORT, so that it can be applied to a simple ultra wideband radar system with a single antenna. This method assumes propagation and scattering for a point-like target, and the decomposing of a matrix calculated in the frequency-domain using SVD. The image is calculated with a method based on the orthogonality between different vector subspaces. The performance of the frequency-domain DORT for a non-point target was investigated. This study calculated the received signals using the FDTD method, assuming a cylindrical metallic target with a radius that was changed from 1.0 mm to 100.0 mm. The resulting images using the data processed by the conventional TR and the frequency-domain DORT were evaluated in terms of accuracy and sharpness.

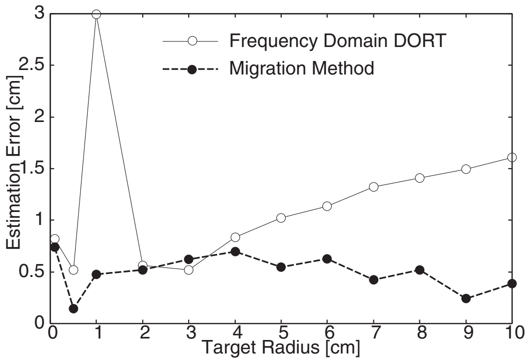

Fig. 5. Estimation error for each method.

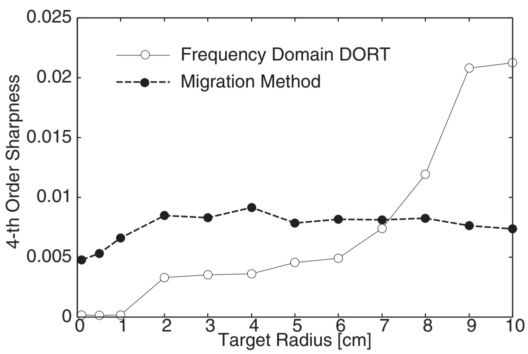

Fig. 6. Sharpness metric for each method.

7. REFERENCES

[1] A. Cresp, I. Aliferis, M. J. Yedlin, C. Pichot and J. -Y. Dauvignac, "Investigation of time-reversal processing for surface-penetrating radar detection in a multiple-configuration," Proc. European Radar Conference, pp. 144, 2008.

[2] A. J. Devaney, "Time reversal imaging of obscured targets from multistatic data," IEEE Trans. Antennas and Propagt., vol. 53, no. 5, May 2005.

[3] D. M. Fromm, C. F. Gaumond, J. F. Lingevitch, R. Menis, D. C. Calvo, G. F. Edelmann, E. Kim, "The effect of coherence and noise on the decomposition of the time reversal operator," Proc. MTS/IEEE OCEANS, pp. 1210–1215, 2005.

[4] P. Simko, J. Saniie, "Computational time reversal ultrasonic array imaging of multipoint targets," Proc. IEEE ultrasonic symposium, pp. 1208–1212, 2007.

[5] T. Sakamoto and T. Sato, "Time-reversal UWB imaging with a single antenna in multi-path environments," 3rd European Conference on Antennas and Propagation (EuCAP), pp. 2177–2181, 2009.

[6] R. A. Muller and A. Buffington, "Real-time correction of atmospherically degraded telescope images through image sharpening," J. Optical Society of America, vol. 64, no. 9, pp. 1200-1210, 1974.